J Therm Anal Calorim (2015) 121:1225–1232
DOI 10.1007/s10973-015-4586-0

Thermal properties of $60P_2O_5$–$20Fe_2O_3$–$20Al_2O_3$ glass for salt waste immobilization

Malgorzata Ciecińska · Paweł Stoch · Agata Stoch · Marek Nocuń

Received: 31 December 2014 / Accepted: 16 February 2015 / Published online: 1 April 2015

Abstract Vitrification is the most effective method of hazardous waste immobilization. Toxic elements are incorporated into a glass structure. Iron alumino-phosphate glasses are presently being considered as a matrix for storage of a radioactive waste which cannot be vitrified using conventional borosilicate waste glasses. Influence of Na_2SO_4 as a one of components such the waste on thermal properties and crystallization ability of $60P_2O_5$–$20Fe_2O_3$–$20Al_2O_3$ glass was studied. It was observed that Na_2SO_4 decreases transformation temperature and increases ΔC_p. The glass characteristic temperatures, glass crystallization ability and crystallizing phases were determined. Na_2SO_4 increases the glass crystallization ability which could be related with ΔC_p heat capacity accompanying glass transition changes. The glass internal structure rebuilding accompanying the sodium content increase is considered. The obtained results were compared with structural model previously developed for $60P_2O_5$–$40Fe_2O_3$ glass and showed the structural similarity between these glasses.

Keywords Iron alumino-phosphate glass · Thermal analysis · Thermal properties · Nuclear waste · Vitrification

M. Ciecińska · P. Stoch (✉) · M. Nocuń
Faculty of Material Science and Ceramics, AGH-University of Science and Technology, Mickiewicza 30 Ave., 30-059 Kraków, Poland
e-mail: pstoch@agh.edu.pl

A. Stoch
Institute of Electron Technology Krakow Division, Zablocie 39, 30-701 Kraków, Poland

Introduction

Vitrification is the most effective method of the hazardous waste immobilization. Toxic elements are incorporated into glass structure. Borosilicate glasses are of common use in nuclear waste immobilization procedure. Lately, glasses from Fe_2O_3 to P_2O_5 system are of the great interest, for scientific reason and because they are considered as a high-capacity matrix for storage of radioactive waste [1, 2]. The worldwide used borosilicate glasses for nuclear waste vitrification are not suitable for immobilization of high content molybdenum, chromium or salt waste because of the low solubility of these compounds in the borosilicate glass. However, most phosphate glasses have a low chemical durability [3–5], but iron as a glass component significantly increases it. The highest chemical durability has among others $60P_2O_5$–$40Fe_2O_3$ (Fe/P = 0.67) glass. All of them have an O/P ratio of over 3 and are classified as polyphosphate glasses [6]. There are indications that iron strengthens the chemical bonds in the glass structure making their properties comparable or even better than those of borosilicate [1, 2].

Besides their excellent chemical durability, iron phosphate glasses have the melting temperature about 100–200 K lower than borosilicate glass, and also due to lower viscosity of the melts, their homogenization time is more than 4 times shorter [7].

Iron phosphate glasses are now considered for a vitrification of waste containing relatively high concentration of actinide elements, high concentration of sodium, caesium sulphate and chloride, chloride waste from pyrochemical reprocessing of Pu metal and waste containing various metals, radioactive ceramics, polymers or carbon [1, 8, 9].

The local structure of iron in these glasses is complicated by the fact that depending on conditions of the

synthesis, and the glass may contain variable amounts of Fe^{2+} ions. It leads to extremely complex crystallography of the iron phosphate system which is composed of over 20 different crystalline phases in which iron can be present in both valence states and coordination numbers to oxygen from 4 to 6. Several structural models of the iron phosphate glasses exist in literature [10–13].

It is worth to mention that in iron phosphate glasses, part of iron is always in ferrous state with its amount depending on the synthesis conditions from about 10 to even 100 %. On the other hand, during studies on immobilization of caesium, there were obtained glasses with almost only ferric iron but with some Cs_2O content. The structure of these glasses does not change with Cs_2O content up to about 22 mol%, but above this threshold some structural changes are observed [14, 15]. Analogously, investigations on immobilization of Na_2SO_4 in similar glasses showed an increase in stability of the glass structure up to about 30 mol% and rebuilding it for higher contents of Na_2O [16].

Taking all of these into account, in the present paper the influence of Na_2SO_4 as a one of the salty waste components on the thermal properties and glass stability against crystallization of $60P_2O_5$–$20Fe_2O_3$–$20Al_2O_3$ glass were studied. The structural aspects of the high capacity of salt waste incorporation are considered as well.

Experimental

Glass containing 20 mol% Fe_2O_3, 20 mol% Al_2O_3 and 60 mol% P_2O_5 was prepared from chemical pure $NH_4H_2PO_4$, Fe_2O_3 and Al_2O_3. Approximately 20 mass% overweight of $NH_4H_2PO_4$ was used to compensate P_2O_5 losses during melting of the batch due to evaporation [17]. Batches were melted for 2 h at 1473 K in Al_2O_3 crucible in an electric furnace with the furnace atmosphere as close to natural as possible. The melt was vitrified by casting onto steel plate and crushed into 0.3–0.1 mm grain size. Chemical composition of the obtained glass was check by XRF method, and in experimental error, limit range was the same as assumed. The glass frit was mixed with Na_2SO_4 (used as a waste simulator) and remelted at 1473 K for 2 h. Na_2SO_4 to the glass ratio was $x = 10, 20, 30, 40, 50$ mol%. The glasses were prepared in the similar conditions like in [16, 18] which could lead to assumption that approximately 30 % of iron was reduced to Fe^{2+} [18]. Samples were designated as PFAS10, PFAS20, PFAS30, PFAS40 and PFAS50, respectively (Table 1).

Heating microscopy thermal analysis was carried out using compacted powder samples of cubic shape. Powdered samples prepared by milling of bulk samples in a ball mill were wetted in ethanol and compacted to cubes of $3 \times 3 \times 3$ mm by a hand press. The changing of the samples shape was conducted by Carls Zeiss MH01 microscope at heating rate of 10 K min^{-1}. Data of the sample height were collected at intervals of 10 K during the experiment, and shrinkage curves were obtained. The beginning of sintering process temperature T_s as the onset of densification was determined from the shrinkage curve. The half sphere temperature T_{hs} which was the temperature at which the height of the sample was half the width of the base and the flow temperature T_f which was the first temperature at which the sample is melted to a third of its original height were observed.

Table 1 Chemical composition of the glasses/mol%

Oxide	PFAS10	PFAS20	PFAS30	PFAS40	PFAS50
P_2O_5	54	48	42	36	30
Fe_2O_3	18	16	14	12	10
Al_2O_3	18	16	14	12	10
Na_2SO_4	10	20	30	40	50

Glass transformation temperature T_g at the half of the heat capacity step on DSC curve, crystallization T_c as the onset of the first crystallization peak and liquidus T_L as the onset of the first melting peak temperature were measured by differential scanning calorimetry (DSC) method at the heating rate of 10 K min^{-1}. Measurements were carried out using Netzch STA 449 F1 Jupiter, operating in the heat flux DSC mode. Powdered glass samples weighing 60 mg were heated in Al_2O_3 crucibles at a rate of 10 K min^{-1} in a dry air atmosphere up to 1350 K. Characteristic temperatures of the glass transformation effects and changes of specific heat at T_g were determined applying the Netzsch Proteus Thermal Analysis Program (version 5.0.0.).

Crystallization of the glasses was checked by heating the powdered samples by 2 h at T_c temperature of exothermic DSC peak. Phase composition of the samples was investigated by X-ray diffractometry (XRD) using DRON 1.5 apparatus and Cu $K\alpha$ radiation, and the measured spectra were analysed using X'Pert HighScore Plus software. The obtained spectra were fitted using Rietveld method, and semi-quantitative analysis of crystallizing phases were done.

Results

Heating microscopy of the glass waste mixtures

The sintering and the half sphere temperatures of the glass waste mixtures were determined using heating microscopy. The measured shrinkage curves are presented in Fig. 1, and the obtained temperatures are collected in Table 2.

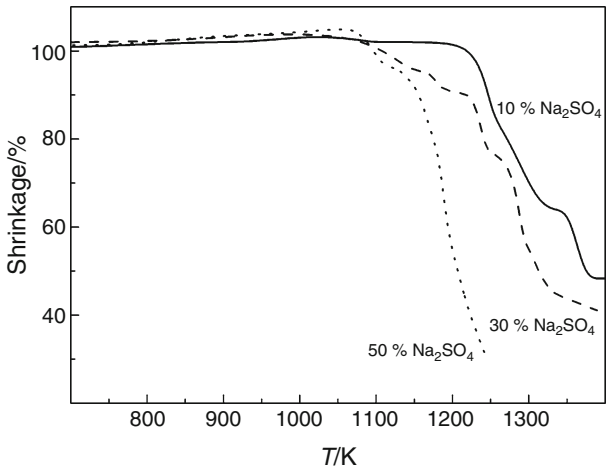

Fig. 1 Shrinkage curves of the glass and Na_2SO_4 mixtures

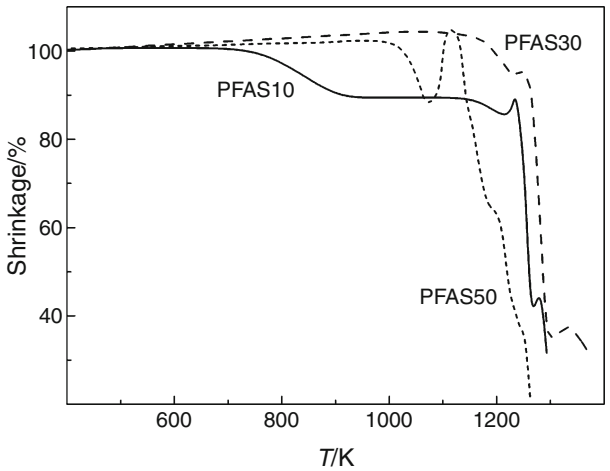

Fig. 2 Shrinkage curves of the PFAS10, PFAS30 and PFAS50 glasses

Table 2 Sintering T_s and half sphere T_{hs} temperatures of the glass and Na_2SO_4 mixtures

Na_2SO_4 content/mol%	T_s/K	T_{hs}/K
10	1220(10)	1380(10)
20	1180(10)	1360(10)
30	1075(10)	1313(10)
40	1060(10)	1240(10)
50	1070(10)	1210(10)

The mixtures start sintering about 1200 K, and increase in the simulated waste content decreases the sintering temperature even to about 1100 K. The melting process starts over 1400 K for low waste content and is considerably decreased to about 1200 K for the high waste loadings.

Heating microscopy of the glasses

The sintering, the half sphere and the flow temperatures of the studied glasses were determined using heating microscopy. The measured shrinkage curves are presented in Fig. 2, and the obtained characteristic temperatures are collected in Table 3.

It is interesting to notice that all the characteristic temperatures are increased with Na_2SO_4 up to 30 mol%, and then, the opposite effect is observed.

DSC analysis of the glasses

The effect of addition of the Na_2SO_4 to the iron aluminophosphate glass on its thermochemical properties is demonstrated by the DSC curves. An exemplary DSC curve for the samples containing 10, 30 and 50 mol% of sodium sulphate is presented in Fig. 3.

Table 3 Sintering T_s and half sphere T_{hs} and flowing T_f temperatures of the glasses

Glass	T_s/K	T_{hs}/K	T_f/K
PFAS10	740(10)	1220(10)	1290(10)
PFAS20	770(10)	1260(10)	1340(10)
PFAS30	1140(10)	1290(10)	1370(10)
PFAS40	975(10)	1280(10)	1330(10)
PFAS50	1023(10)	1220(10)	1260(10)

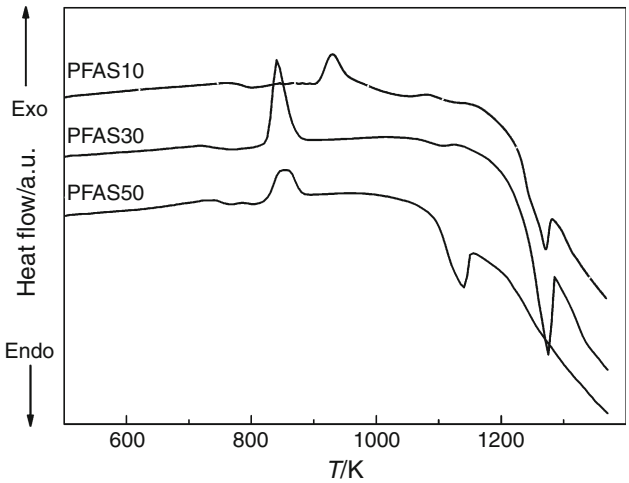

Fig. 3 DSC curves of the PFS0, PFS20 and PFS50 samples

All the samples show the transformation step which is increasing with Na_2SO_4 content and follows to the increase in the value of molar heat capacity change ΔC_p accompanying the glass transformation. Just behind there appears an exothermic effect of crystallization which is being stronger

Table 4 Transformation (T_g), crystallization (T_c), liquidus (T_L) temperatures, ΔC_p, Hruby's parameter (K_H)

Sample	T_g/K	T_c/K	T_L/K	ΔC_p/J g^{-1} K^{-1}	K_H
PFAS10	775(5)	907(5)	1272(5)	0.257(9)	0.362
PFAS20	768(5)	898(5)	1277(5)	0.263(9)	0.342
PFAS30	743(5)	827(5)	1275(5)	0.314(9)	0.187
PFAS40	733(5)	819(5)	1227(5)	0.362(9)	0.211
PFAS50	723(5)	813(5)	1140(5)	0.404(9)	0.275

when sodium is added, and the highest peak is observed for the PFAS30 sample. Further increasing of Na_2SO_4 content leads to decrease in the crystallization effect. After the crystallization peak, melting of the glasses occurs as an endothermic effect on the corresponding DSC curves. The similar curves are observed for the rest of the measured samples. The transformation, crystallization and melting temperatures of the investigated materials are presented in Table 4.

Influence of the Na_2SO_4 content on transformation temperature T_g and the molar heat capacity ΔC_p accompanying the glass transformation is presented in Fig. 4.

The T_g temperature is linearly decreased, and the ΔC_p value is growing linearly with increasing sodium content in the glass (Fig. 4.).

The Na_2SO_4 incorporation leads to growth of Na_2O content and increases the change in the specific heat capacity ΔC_p accompanying the glass transformation (Fig. 4b). As was mentioned previously [19, 20], ΔC_p value can be an indicator of a degree of the structural changes accompanying the transformation, such as number and strength of the broken bonds and rearrangement of structure constituents. The ΔC_p value is related to the change in entropy accompanying glass transition and at the same as the structure rebuilding degree indicator [21].

One of the important parameters in case of waste vitrification is a thermal stability of a vitrified product. There exists in a literature number of different glass stability criterions, e.g. [22–26], and a nice comparison between them for iron phosphate glasses is given in [27], and most of those criterions show the similar dependence on glass composition. In case of iron phosphate glasses, one of the most frequently used is Hruby criterion, and therefore, the glass stability of the investigated materials was evaluated using it [16, 27]. According to [22], the higher K_H value, the greater would be its stability against crystallization. The K_H values were evaluated according to the formulae:

$$K_H = \frac{T_c - T_g}{T_L - T_c} \quad (1)$$

The obtained K_H parameters are summarized in Table 4 and Fig. 5.

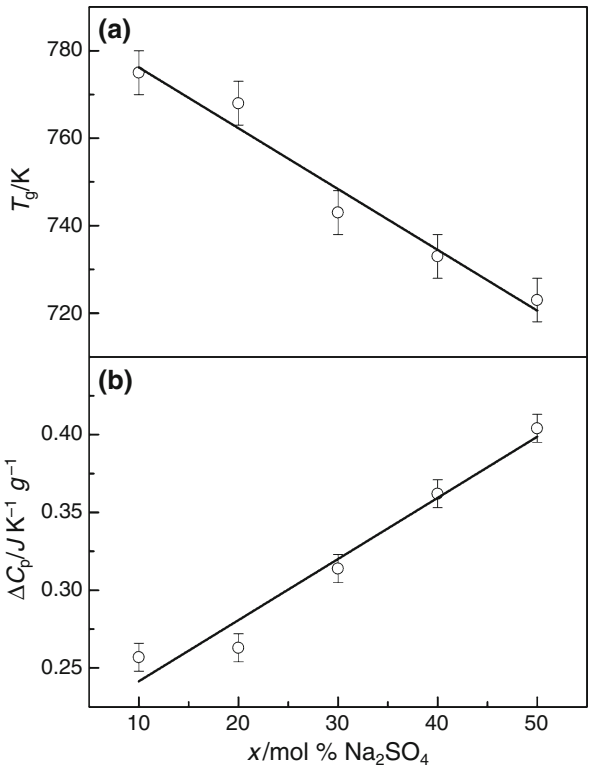

Fig. 4 Transformation temperature T_g (**a**) and the molar heat capacity ΔC_p accompanying the glass transformation (**b**) as function of the Na_2SO_4 content (mol%)

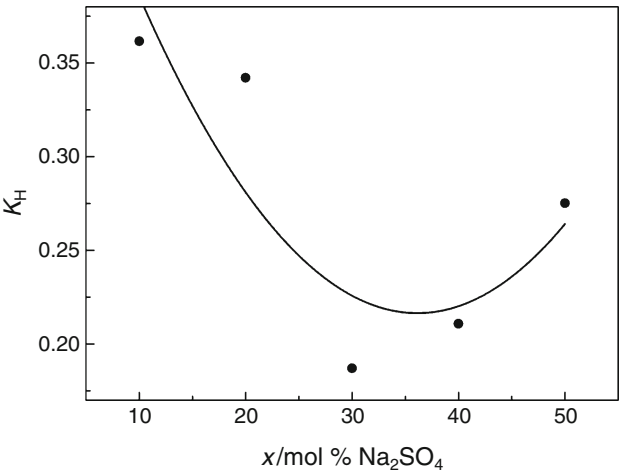

Fig. 5 Hruby parameter K_H as Na_2SO_4 content function

All of the investigated glasses evidenced a quite good thermal stability comparable with conventional silicate glasses for which K_H value varied from 0.14 to about 1.3 [16, 27–30]. The increasing Na_2SO_4 addition causes decrease in the K_H parameter which means lowering the glass stability against crystallization and at the same ability of glass to vitrify on cooling [30]. The lowest K_H value is

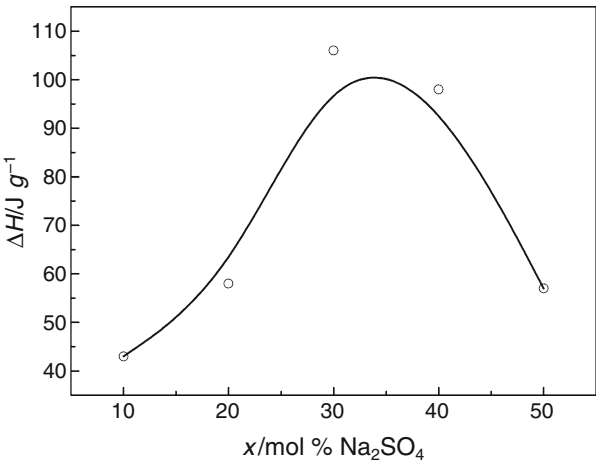

Fig. 6 Enthalpy of the crystallization of glasses (ΔH) as dependent on the Na_2SO_4 (mol%) content

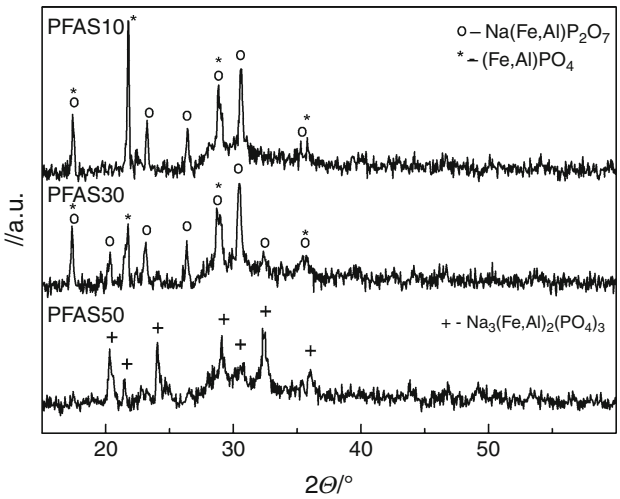

Fig. 7 XRD patterns of compounds crystallizing in the PFAS10, PFAS30 and PFAS50 glasses

observed for the glass with 30 mol% of Na_2SO_4. Further increasing of sodium sulphate content increases the K_H parameter.

Enthalpy of crystallization calculated from DSC curves exothermic peak area is growing up rapidly with Na_2SO_4 content, but above $x = 30$ mol% is falling down (Fig. 6) which could suggest the change in the crystallization mechanism above the Na_2SO_4 30 mol% content.

XRD analysis

The XRD patterns of the compounds crystallizing in PFAS10, PFS30 and PFS50 glasses at T_c temperature indicated by the DSC are presented in Fig. 7 and Table 5.

Two main crystalline phases formed in the glasses of low concentration of sodium are berlinite type $(Fe,Al)PO_4$ phase and sodium-containing compound $Na(Fe,Al)P_2O_7$. The second phases crystallize at the cost of $(Fe,Al)PO_4$ whose quantity decreases with increasing Na_2SO_4 content and disappears for sodium sulphate content higher than 30 mol%. Further increasing sodium concentration leads to crystallization of sodium-rich phase such as $Na_3(Fe,Al)_2(PO_4)_3$.

Generally, in iron phosphate glasses, composition of the crystallizing compounds depends on the glass composition, heat treatment, atmosphere in furnace and the Fe^{2+}/Fe^{3+} ratio. Phases formed in the glasses investigated here are similar to those observed in case of crystallization caesium [14] and sodium iron phosphate glasses [16–18]. It should be also noticed here that in case of high concentration of Na_2SO_4 in the glass (above 30 mol%), the crystallization peak (Fig. 3) is complex indicating that more stages of glass structure rebuilding take place during the glasses crystallization. This is supported by previous studies of similar glasses in which change in crystallization mechanism is proposed for high Na_2SO_4 content [16].

Table 5 Compounds crystallizing in the investigated glasses, semi-quantity analysis and ICDD reference codes

Sample	Crystal phase	Semi-quantity/mass%	Ref. code.
PFAS10	$(Fe,Al)PO_4$	34	01-089-5599
	$Na(Fe,Al)P_2O_7$	66	01-080-1476
PFAS20	$(Fe,Al)PO_4$	22	01-089-5599
	$Na(Fe,Al)P_2O_7$	78	01-080-1476
PFAS30	$(Fe,Al)PO_4$	12	01-089-5599
	$Na(Fe,Al)P_2O_7$	88	01-080-1476
PFAS40	$Na(Fe,Al)P_2O_7$	54	01-080-1476
	$Na_3(Fe,Al)_2(PO_4)_3$	46	00-033-1251
PFS50	$Na_3(Fe,Al)_2(PO_4)_3$	100	00-033-1251

Discussion

Based on structural model of $60P_2O_5$–$40Fe_2O_3$, glass is proposed in [13]. The glass is build of small rings of $[PO_4]$ and $[FeO_4]$ tetrahedral which are joined together in a similar way like in crystalline α-$FePO_4$, whose crystal structure is the same as berlinite ($AlPO_4$). The reducing conditions of the melt change a part of ferric iron to ferrous which can lead to breaking some of the rings and changing the role of iron from a network former to a network modifier. In the proposed model, Fe^{2+} ions can behave as typical glass network modifiers joined to non-bridging oxygen atoms and cross-link glass chains and increase the stability of the glass structure [13]. According to the model, the $[FeO_4]$ tetrahedra have unbalanced charge. To compensate it, they can electrostatically bonded monovalent ions like Na^+ what change their role from a glass network modifier to a charge compensator of $[FeO_4]^-$. It was shown that depending on Fe^{3+}/Fe^{2+} ratio, 20–30 mol% of Na_2O is

needed to fully compensate charge of $[FeO_4]^-$ tetrahedra. The charge compensating role of Na^+ or Cs^+ ions increases stability and binding energy of the structural units proposed in the model thus increasing the glass melting temperature with increasing Na_2O content which was observed experimentally [14, 16]. Higher concentration of Na_2O causes that the chains built of the structural units break and separate themselves, which can be observed as a rebuilding of the glass structure [13].

In the chain structure of metaphosphate Na_2O–Al_2O_3–P_2O_5 glasses, Al^{3+} has *CN* 6 and together with Na^+ alternatively saturates the charge of the non-bridging oxygen's in the phosphate chains. Similar Al and Na arrangements appear in pyrophosphates glasses from this system. In the orthophosphate glass structure, $[PO_4]$ tetrahedron is saturated by two Al^{3+} ions with the *CN* 4, and one with *CN* 6 and plus one cation Na^+. With the Al_2O_3 content increase, the content of alumina in coordination 4 and orthophosphate $[PO_4]$ groups increases accordingly [31]. When the ratio Al_2O_3/P_2O_5 exceeds 0.63, glass network is made up mainly by the $[AlO_4]$ and $[PO_4]$ tetrahedra, joined each other by the bridging oxygen's—mixed alumino-phosphate network [32].

It is quite surprising that increasing Na_2SO_4 content in the glass melting temperature (Table 4) is almost constant, and half sphere temperature (Table 3) is even slightly increasing up to approximately 30 mol% of sodium sulphate. Higher content of the simulated waste leads to decrease both of these temperatures. It could suggest that similarly for $60P_2O_5$–$40Fe_2O_3$ glass, Na^+ cations are first of all charge compensators of $[FeO_4]^-$ or $[AlO_4]^-$ tetrahedra. If we assume that in case of $60P_2O_5$–$20Fe_2O_3$–$20\ Al_2O_3$ glass, a similar structural model is valid like for the $60P_2O_5$–$40Fe_2O_3$ and half of the $[FeO_4]^-$ tetrahedra is replaced by $[AlO_4]^-$ than we shall expect that full compensation of $[FeO_4]^-$ and $[AlO_4]^-$ tetrahedra will take place for the PFAS30 glass in which the simulated waste loading is equal 30 mol%. For the higher waste content in the glass, Na^+ cations are changing their role from the charge compensators to the glass network modifiers and start breaking the chains build of the structural units proposed in [13]. Thus, up to 30 mol% of Na_2SO_4, the melting and the half sphere temperatures are not decreasing, and above this threshold, when the role of sodium is changing, both of these temperatures are decreasing.

Influence of Na_2SO_4 content on transformation temperature T_g is presented in Fig. 4a. The T_g temperature is reduced with the simulated waste addition which is causing decreasing the number of network forming cations which leads to reduction in the directional covalent bonds and at the same time increase the proportion of ionic bonds. Increasing the number of ionic bonds indicates that the structure becomes more flexible, and cations could move easier thus leading to reduction in the T_g [19, 33].

As was mentioned above, introduction of Na_2SO_4 to the glass structure reduces the number of covalent bonds. These bonds because of its directional nature could lead to higher internal structural strains. The strains may cause the cracking of the bonds, which is less probable in the case of bonds of high ionicity. More the internal strain, the higher energy is accumulated in the glass network and lower energy is needed to break the bonds at the glass transition temperature [33]. It is supported by the fact that the transition of pure silicate glasses takes place with the very small change in C_p [20]. Thus, increase in ΔC_p with Na_2SO_4 (modifiers) concentration is observed (Fig. 4b). The heat capacity changes in the glass transition region could be a kind of measure of fragility of the glass. Strong liquids usually show smaller changes of ΔC_p than fragile liquids [34, 35]. The observed ΔC_p changes (Fig. 4b) indicate that the fragility of the glass increases with increasing Na_2SO_4 content and is in a good agreement with weakening of chemical bonds in the glass structure reflected by a decrease in glass transition temperature (Fig. 4a) [35]. The higher fragile glasses are characterized by higher viscosity of the melt [36, 37].

According to the model discussed above, $60P_2O_5$–$40Fe_2O_3$ glass is build of structural units which are composed of three $[PO_4]$ and two $[FeO_4]$ tetrahedra, Fe^{2+} cations which are charge compensators of $[FeO_4]^-$ and some additional $[PO_4]$ tetrahedra whose number depends on Fe^{2+}/Fe^{3+} ratio. Crystallization of this glass leads to formation of berlinite type α-$FePO_4$ phase and $Fe_2P_2O_7$ [16, 38]. According to XRD results in the investigated glasses at small Na_2SO_4 content, below 30 mol% crystallization of similar phase is observed like berlinite type $(Al,Fe)PO_4$ and $Na(Fe,Al)P_2O_7$ whose content is increasing (Table 5). At crystallization temperature, rearrangement of the structural units takes place. The charge compensated $Na[Fe/AlO_4]$ tetrahedra are joined to two $[PO_4]$, and $Na(Fe,Al)P_2O_7$ is formed. The rest of $[Fe/AlO_4]$ and $[PO_4]$ tetrahedra share their vertices with each other and form even membered rings the same like in $(Al,Fe)PO_4$ crystals [12, 13]. There was no observed crystallization of phases containing Fe^{2+} which is almost always present in iron phosphate glasses [39, 40]. According to thermogravimetric results, which are not shown here, at crystallization temperature there is a observed small mass increase (approximately 0.3 %) for all of the investigated glasses. This small increase could be related to oxidation of iron from ferrous to ferric. For the higher concentration of Na_2SO_4 formation of sodium-rich phase, $Na_3(Fe,Al)_2(PO_4)_3$ is detected. In the above structural model, changing sodium role from a charge compensator to a network modifier leads to brake of the chains building of the mentioned above units. To fully separate one structural unit, three Na^+ cations are needed. The

separated element is build of three Na, two Fe/Al and three P atoms, and thus, formation of $Na_3(Fe,Al)_2(PO_4)_3$ can take place. Concluding the XRD analysis results confirmed the structural similarity of $60P_2O_5$–$40Fe_2O_3$ glass to $60P_2O_5$–$20Fe_2O_3$–$20Al_2O_3$.

Form vitrification point of view, very important factors are glass waste mixtures melting temperature and stability against crystallization of the obtained glass. The glass waste mixtures start melting at temperatures which are much below 1500 K which can make them suitable for vitrification of volatile elements such as Cs. On the other hand, the K_H parameter is at acceptable level but much below the level for borosilicate waste glasses which is in the range 0.8–1.3 [33], and especially for the PFAS30 glass ($K_H = 0.187$), there exists possibility of formation of crystalline inclusions. Partial crystallization of the product could be difficult to avoid during vitrification of radioactive waste when the melt is poured into big drums, and cooling rate of the melt is rather low. The highest degree of glass crystallization is obtained for the PFAS30 glass for which the K_H value is the lowest and enthalpy of crystallization is the highest (Fig. 6). Comparing Figs. 5 and 6, it could be observed relation between K_H value and enthalpy of crystallization ΔH. The highest thermal stability, the lowest the enthalpy of crystallization. Similar phenomena were observed earlier [16, 33].

Conclusions

Thermal properties of $60P_2O_5$–$20Fe_2O_3$–$20Al_2O_3$ (mol%) glass, with increasing content of Na_2O added to it as Na_2SO_4, being the simulator of the radioactive salt waste were investigated. It was demonstrated that the change in the properties with the glass chemical composition being the effect of internal structure rebuilding accompanying the sodium content increases.

It was shown based on thermal properties and crystal phases formation during the glasses crystallization, the structural role of sodium can change from the charge compensator of $[FeO_4]$ and $[AlO_4]$ tetrahedra to the glass network modifier.

The obtained results confirmed the structural similarity of the investigated glass to the $60P_2O_5$–$40Fe_2O_3$.

Acknowledgement The work was done at Faculty of Materials Science and Ceramics AGH-University of Science and Technology in Krakow in 2014 year within statutory research no 11.11.160.365.

References

1. Donald W. Immobilisation of radioactive and non-radioactive wastes in glass-based systems: an overview. Glass Technol. 2007;48:155–63.
2. Ojovan MI, Lee WE. An Introduction to nuclear waste immobilisation. 1st ed. Oxford: Elsevier; 2005.
3. Szumera M, Wacławska I, Olejniczak Z. Influence of B_2O_3 on the structure and crystallization of soil active glasses. J Therm Anal Calorim. 2010;99:879–86.
4. Szumera M, Wacławska I. Effect of molybdenum addition on the thermal properties of silicate–phosphate glasses. J Therm Anal Calorim. 2012;109:649–55.
5. Wacławska I, Szumera M, Stoch P, Sitarz M. Structural role of Fe in the soil active glasses. Spectrochim Acta Part A Mol Biomol Spectrosc. 2011;79:728–32.
6. Brow RK. Review: the structure of simple phosphate glasses. J Non Cryst Solids. 2000;263&264:1–28.
7. Kim CW, Day DE. Immobilization of Hanford LAW in Iron phosphate glasses. J Non Cryst Solids. 2003;331:20–31.
8. Bingham PA, Hand RJ, Scales CR. Immobilisation of simulated plutonium—contaminated material in phosphate glasses: an initial scoping study. Mater Res Soc Symp Proc. 2006;932:345–52.
9. Stoch P, Ciecinska M. Thermochemistry of phosphate glasses for immobilization of dangerous waste. J Therm Anal Calorim. 2012;108:705–9.
10. Wedgwood FA, Wright AC. Short range antiferromagnetic ordering in vitreous Fe_2O_3–P_2O_5. J Non Cryst Solids. 1976;21:95–105.
11. Marasinghe GK, Karabulut M, Ray CS, Day DE, Shumsky MG, Yelon WB, Booth CH, Allen PG, Shuh DK. Structural features of iron phosphate glasses. J Non Cryst Solids. 1997;222:144–52.
12. Wright AC, Sinclair RN, Shaw JL, Haworth R. The atomic and magnetic structure and dynamics of iron phosphate glasses. Phys Chem Glasses. 2012;53:227–44.
13. Stoch P, Szczerba W, Bodnar W, Ciecinska M, Stoch A, Burkel E. Structural properties of iron-phosphate glasses spectroscopic studies and ab initio simulations. Phys Chem Chem Phys. 2014;16:19917–27.
14. Joseph K, Ghosh S, Govindan Kutty KV, Vasudeva Rao PR. Crystallization kinetics, stability and glass forming ability of iron phosphate and cesium loaded iron phosphate glasses. J Nucl Mater. 2012;426:233–9.
15. Joseph K, Govindan Kutty KV, Chandramohan P, Vasudeva Rao PR. Studies on the synthesis and characterization of cesium-containing iron phosphate glasses. J Nucl Mater. 2009;384:262–7.
16. Stoch P, Ciecinska M, Stoch A. Thermal properties of phosphate glasses for salt waste immobilization. J Therm Anal Calorim. 2014;117:197–204.
17. Ray CS, Fang X, Karabulut M, Marasinghe GK, Day DE. Effect of melting temperature and time on iron valence and crystallization of iron phosphate glasses. J Non Cryst Solids. 1999;249:1–16.
18. Stoch P, Stoch A. Mössbauer spectroscopy study of $60P_2O_5$–$40Fe_2O_3$ glass crystallization. Nukleonika. 2015;60:131–4.
19. Stoch L, Wacławska I, Środa M. Thermal study of the influence of chemical bond iconicity on the glass transformation in (Na_2O, CaO, MgO)–Al_2O_3–SiO_2 glasses. J Therm Anal Calorim. 2004;77:57–63.
20. Stoch L. Thermochemistry of solids with flexible structures. J Therm Anal Calorim. 1998;54:9–24.
21. Stoch L. Thermal analysis and thermochemistry of vitreous to crystalline state transition. J Therm Anal Calorim. 2004;77:7–16.

22. Hruby A. Evaluation of glass-forming tendency by means of DTA. Czech J Phys B. 1972;22:1187–96.
23. Malek J. Thermal stability of chalcogenide glasses. J Therm Anal Calorim. 1993;40:159–70.
24. Cooper EI, Angell CA. Far-IR transmitting, cadmium iodide-based glasses. J Non Cryst Solids. 1983;56:75–80.
25. Drexhage MG, El-Bayoumi OH, Lipson H, Moynihan CT, Bruce AJ, Lucas J, Fonteneau G. Comparative study of BaF_2/ThF_4 glasses containing YF_3, YbF_3 and LuF_3. J Non Cryst Solids. 1983;56:51–6.
26. Weinberg MC. An assessment of glass stability criteria. Phys Chem Glasses. 1994;35:119–23.
27. Ma L, Brow RK, Ghussn L, Schlesinger ME. Thermal stability of Na_2O–FeO–Fe_2O_3–P_2O_5 glasses. J Non Cryst Solids. 2015;409:131–8.
28. Cabral AA, Cardoso AAD, Zanotto ED. Glass-forming ability versus stability of silicate glasses. I. Experimental test. J Non Cryst Solids. 2003;320:1–8.
29. Lin SE, Cheng YR, Wei WCJ. Synthesis and long-term test of borosilicate-based sealing glass for solid oxide fuel cells. J Eur Ceram Soc. 2011;31:1975–85.
30. Nascimento MLF, Souza LA, Ferreira EB, Zanotto ED. Can glass stability parameters infer glass forming ability? J Non Cryst Solids. 2005;351:3296–308.
31. Brow RK. The nature of alumina in phosphate glass I. Properties of sodium alumino phosphate glass. J Am Ceram Soc. 1993;76:913–8.
32. Jin Y, Jiang D, Chen X, Bian B, Huawy X. Raman spectrum studies of the glasses in the system Na_2O–Al_2O_3–P_2O_5. J Non Cryst Solids. 1986;80:147–51.
33. Ciecinska M, Stoch P, Stoch A. Thermal properties of vitrified LLW hospital waste incineration ash. J Therm Anal Calorim. 2014;116:35–9.
34. Zhu D, Ray CS, Zhou W, Day DE. Glass transition and fragility of Na_2O–TeO_2 glasses. J Non Cryst Solids. 2003;319:247–56.
35. Subcik J, Mosner P, Koudelka L. Thermal behaviour and fragility of Sb_2O_3–containing zinc borophosphate glasses. J Therm Anal Calorim. 2008;91:525–8.
36. Nascimento MLF, Aparicio C. Viscosity of strong and fragile glass-forming liquids investigated by means of principal component analysis. J Phys Chem Solids. 2007;68:104–10.
37. Chovanec J, Chromcikova M, Liska M, Shanelova J, Malek J. Thermodynamic model and viscosity of Ge–S glasses. J Therm Anal Calorim. 2014;116:581–8.
38. Joseph K, Jolley K, Smith R. Iron phosphate glasses: structure determination and displacement energy thresholds, using a fixed charge potential model. J Non Cryst Solids. 2015;411:137–44.
39. Karabulut M, Marasinghe GK, Ray CS, Day DE, Waddill GD, Booth CH, Allen PG, Bucher JJ, Caulder DL, Shuh DK. An investigation of the local iron environment in iron phosphate glasses having different Fe(II) concentrations. J Non Cryst Solids. 2002;306:182–92.
40. Stoch P, Ciecinska M, Zachariasz P, Suwalski J, Gorski L, Wojcik T. Mössbauer spectroscopy study of $60P_2O_5$–$40Fe_2O_3$ glass. Nukleonika. 2013;58:63–6.